Cathepsin L Digestion of Nanobioconjugates upon Endocytosis

Violaine Sée,[†,*] Paul Free,[‡] Yann Cesbron,[‡] Paula Nativo,[‡,§] Umbreen Shaheen,[‡] Daniel J. Rigden,[∥] David G. Spiller,[†] David G. Fernig,[‡] Michael R. H. White,[†] Ian A. Prior,[§] Mathias Brust,[‡] Brahim Lounis,[¶] and Raphaël Lévy[‡,*]

[†]Centre for Cell Imaging, [‡]Liverpool Institute for Nanoscale Science and Technology (LINSET), [§]Physiological Laboratory, [∥]School of Biological Sciences, University of Liverpool, Liverpool L69 7ZB, U.K., and [¶]Centre de Physique Moléculaire Optique et Hertzienne, Université Bordeaux 1 and CNRS, 351 Cours de la Libération, 33405 Talence cedex, France

ABSTRACT Understanding the dynamic fate and interactions of bioconjugated nanoparticles within living cells and organisms is a prerequisite for their use as *in situ* sensors or actuators. While recent research has provided indications on the effect of size, shape, and surface properties of nanoparticles on their internalization by living cells, the biochemical fate of the nanoparticles after internalization has been essentially unknown. Here we show that, upon internalization in a wide range of mammalian cells, biological molecules attached to the nanoparticles are degraded within the endosomal compartments through peptide cleavage by the protease cathepsin L. Importantly, using bioinformatics tools, we show that cathepsin L is able to cleave more than a third of the human proteome, indicating that this degradation process is likely to happen to most nanoparticles conjugated with peptides and proteins and cannot be ignored in the design of nanomaterials for intracellular applications. Preservation of the bioconjugates can be achieved by a combination of cathepsin inhibition and endosome disruption.

KEYWORDS: peptide · self-assembled monolayer · endocytosis · bionanotechnology · nanomedicine · gold nanoparticles · protease

New imaging schemes open up the possibility of routine single nanoparticle trapping tracking and imaging inside living cells.[1−7] To attain this objective, it is necessary to control the delivery and intracellular localization of nanoparticles as well as their long-term biochemical fate. Such particles need to be surface-modified with a carefully controlled molecular capping layer, usually of thiolated ligands, that conveys both stability and functionality.[8] Recent studies have highlighted the effect of size, shape, and functionalization on the cytotoxity[9−14] and rate of endocytosis/exocytosis of nanoparticles.[12,15,16] Unfortunately, very little is known about the evolution of the capping layer before, during, and after the internalization process. A precise understanding of the chemical and biomolecular interactions of this layer with its environment is, however, essential for most applications of nanoparticles as intracellular probes or/and delivery agents. There are indications that thiolated ligands could be lost after internalization through ligand exchange with glutathione or other thiol-containing endogenous biomolecules,[17] which may impose a severe restriction to some applications but could also be elegantly turned into an advantage for the design of nanoparticle-based intracellular delivery systems.[17,18] This class of ligands includes cysteine-terminated peptides, which have been shown to form ideal capping layers for metal nanoparticles,[19−21] quantum dots, as well as a number of other nanomaterials.[22,23]

In this work, we present a detailed study of the cellular uptake and subsequent enzymatic modification of gold nanoparticles conjugated with peptides. We show that endocytosis is followed by proteolytic cleavage of peptide bioconjugates in the endosomes orchestrated by the cathepsin L protease. Bioinformatics analysis predicts that more than a third of human proteins could be cleaved by cathepsin L, which has direct implications for the design of all intracellular sensors based on nanoparticles conjugated with peptides and proteins. We also introduce fluorescence quenching by the metal particles as a quantitative measurement of intracellular proteolytic activity.

RESULTS AND DISCUSSION

Classical methods of delivery, which were initially developed for DNA or proteins, were evaluated for the intracellular delivery of peptide-capped gold nanoparticles into HeLa cells. To assess the efficiency and mechanisms of intracellular delivery, cells were observed by transmission electron microscopy (TEM). In all cases, TEM revealed similar endosomal localization (Supporting Information Figure S1A−C), and we

*Address correspondence to violaine@liverpool.ac.uk, rapha@liverpool.ac.uk.

Received for review June 29, 2009 and accepted August 13, 2009.

Published online September 3, 2009. 10.1021/nn9006994 CCC: $40.75

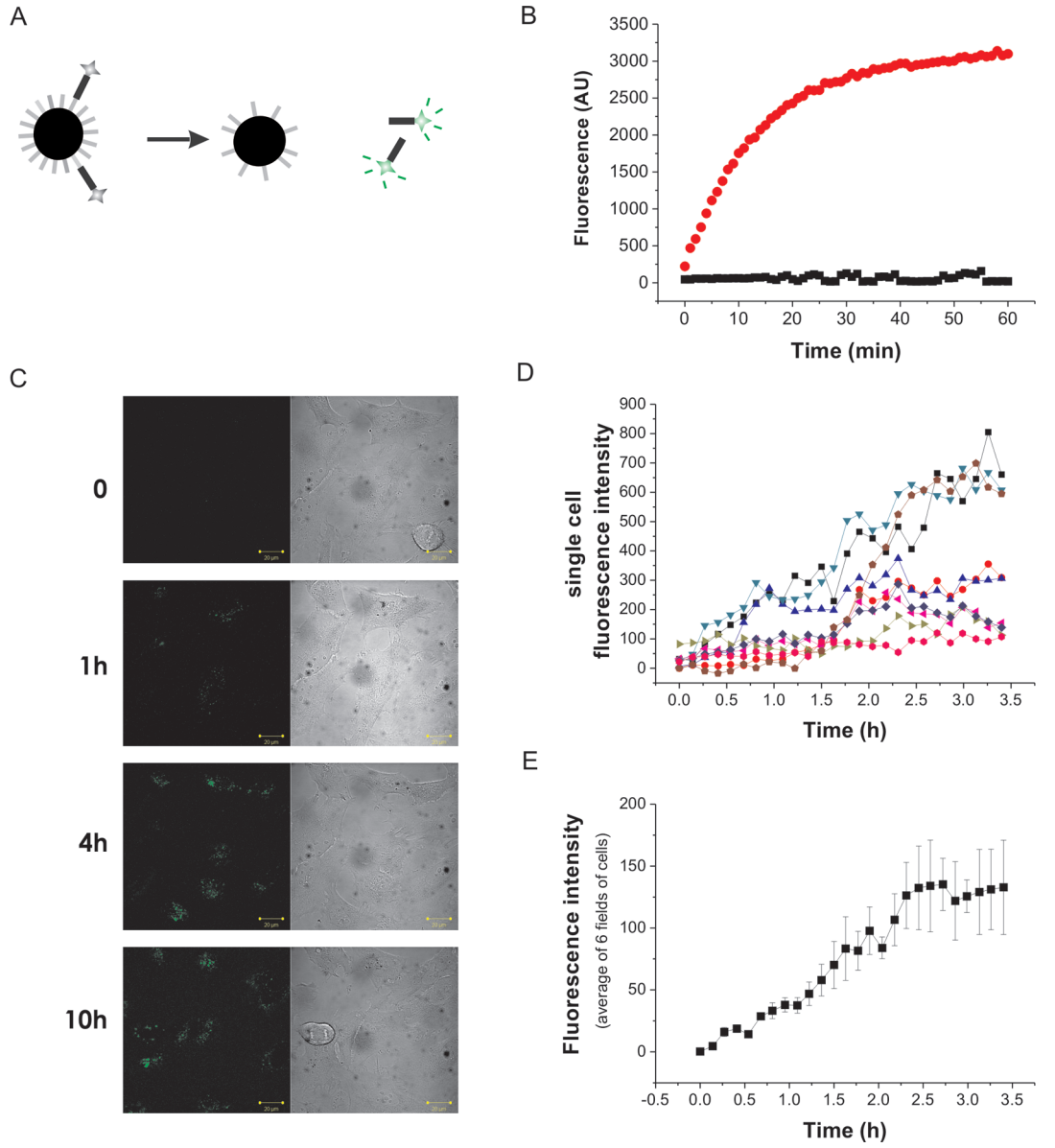

Figure 1. Intracellular fluorescence release upon peptide monolayer degradation. (A) Schematic representation of the experimental principle; 95% CALNN−5% CALNN-*th-fam* gold nanoparticles do not display any fluorescent signal due to quenching by the gold nanoparticles. If the peptide layer is degraded or released from the gold nanoparticles, fluorescence levels increase. (B) *In vitro* assay using thrombin to cleave the FAM group from the gold nanoparticle core and release the fluorescence (red) compared to control conditions without thrombin (black). (C) The 6 nM of 95% CALNN−5% CALNN-*th-fam* gold nanoparticles were incubated onto HeLa cells in the microscope chamber (37 °C, 5% CO_2). Time-lapse images of 10 different fields were taken every 5 min using a Zeiss lsm 510 laser scanning confocal microscope. For each picture, the left panel shows fluorescence images and the right panel shows brightfield images at indicated time. (D) Quantification of fluorescence intensity in nine single cells over 3.5 h incubation. (E) Average of mean fluorescence intensity of 200 single cells as a function of nanoparticle incubation time.

therefore used a simple incubation of the nanoparticles in complete medium for this study. To assess the biochemical stability of the peptide layer in the intracellular compartment, nanoparticles bearing a peptide epitope (FLAG) were prepared and the presence of the epitope was then detected by immunofluorescence. Although FLAG-bearing nanoparticles could be detected on the extracellular membrane, no fluorescence could be detected inside the cells (Supporting Information Figure S1E,F), whereas TEM showed a clear internalization of the nanoparticles (Supporting Information Figure S1A−C). This indicates that the FLAG sequence is degraded or lost during or after internalization. To examine in real-time the chemical fate of the peptide monolayer, we designed a probe based on gold nanoparticle distance-dependent fluorescence quenching (Figure 1A).[24−26] Gold nanoparticles were capped with a mixed monolayer of CALNN (97%) and of a longer fluorescein-containing peptide CALNN-*th-fam* (3%). The latter peptide starts with the CALNN sequence, followed by the protease thrombin cleavage site (LVPRGS), and functionalized with fluorescein on its C-terminal

end. When CALNN-*th-fam* is intact and linked to the nanoparticle, the fluorescence is quenched because of nonradiative energy transfer from the fluorophore to the nanoparticle core.[24,25] The thrombin site was included to enable control *in vitro* experiment. These experiments confirmed that releasing the fluorophore by thrombin cleavage induced a marked increase of fluorescence (Figure 1B).

Time-lapse confocal microscopy in living cells reveals an increase of intracellular fluorescence over time in single living cells after addition of the nanoparticles in the medium, indicating uptake by the cells and subsequent release of the fluorophore (Figure 1C and movie 1 in the Supporting Information). Thrombin, an extracellular enzyme, is not thought to be present in its active form inside these cells. Incubation of the nanoparticles in cell medium only (with 10% serum) does not induce fluorophore release (Supporting Information Figure S2). Quantification of the fluorescence increase was performed at a single cell level and showed some variability in the efficiency of uptake but similar kinetics of uptake for each single cell (Figure 1D,E). The average quantification of ~200 cells showed a strong increase during the first 3 h followed by a plateau. The uptake of 5 nm gold nanoparticles has been followed by the same method and displayed similar kinetics of intracellular uptake (Supporting Information Figure S3).

To characterize the nature of the intracellular vesicles in which peptide degradation occurred and fluorescence accumulated, we stained the acidic vesicles using the lysotracker dye (after 3 h nanoparticle incubation). Surprisingly, we did not observe a complete co-localization of fluorescence, suggesting that not all of the nanoparticles were in acidic vesicles (Figure 2A). We then aimed to disrupt acidic endosomes using chloroquine, an ion-transporting ATPase inhibitor that disrupts endosomes by preventing their acidification.[27] This has previously been described for antisense and nanopartice delivery.[28,29] Electron microscopy shows that, after 3 h nanoparticle incubation in presence of chloroquine, cells displayed disrupted endosomes as well as nanoparticles floating out of the vesicles (Supporting Information Figure S4). A 2.5 time reduction of fluorescence was observed in the presence of chloroquine, indicating a decrease in the degradation of the monolayer when the endosomes are disrupted (Figure 2C,D). Some TEM images showed nanoparticles trapped in multiple-membrane vesicles. Such vesicles are typical of autophagy, a process by which the cell sequesters and subsequently degrades its own components. Recent research indicates that nanoparticles are potent autophagy activators and that autophagic flux is an underlying physiological process of the cellular clearance of the nanoparticles.[30] We therefore incubated the particles in presence of 3-methyladenine, a specific inhibitor of autophagy. We observed a 1.8 time diminution of fluorescence levels

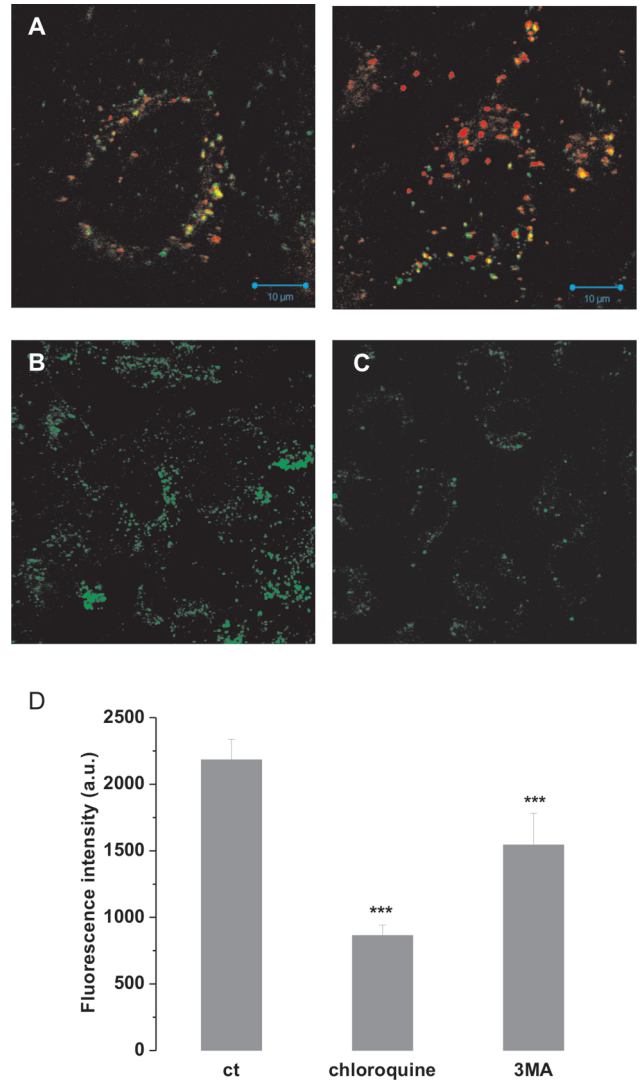

Figure 2. Disruption of intracellular acidic compartments decreases peptide monolayer degradation in living cells. (A) HeLa cells were incubated 3 h in presence of 6 nM of 95% CALNN−5% CALNN-*th-fam* gold nanoparticle (green fluorescence). Cells were then loaded for 15 additional minutes with 37 nM DND-99 lysotracker (red fluorescence). After three washes, confocal images were taken using a Zeiss lsm 510 confocal microscope. (B,C) Cells were incubated for 4.5 h with 6 nM 95% CALNN−5% CALNN-*th-fam* gold nanoparticles in the absence (B) or presence of 100 µM chloroquine (C). (D) Quantification using Kinetic tracker software of a number of fluorescent vesicles observed in B,C and in cells incubated with the same nanoparticles in the presence of 10 mM 3-methyladenine, an autophagy inhibitor; * indicates a statistical difference with $p < 0.01$.**

(statistically significant, $p < 0.01$), suggesting that some autophagy takes place during maturation of the endosomes (Figure 2E). Taken together, these results clearly show that CALNN-capped nanoparticles are entering cells *via* endocytosis and that degradation of the peptide layer occurs inside the endosomes.

We tested human and mouse cell lines as well as adherent and non-adherent cells showing that peptide-capped nanoparticles enter all of these cell lines and that the accompanying degradation is a general phenomenon (Figure 3A). Surprisingly, one of the cell lines (DAOY cells) had a very strong level of fluorescence

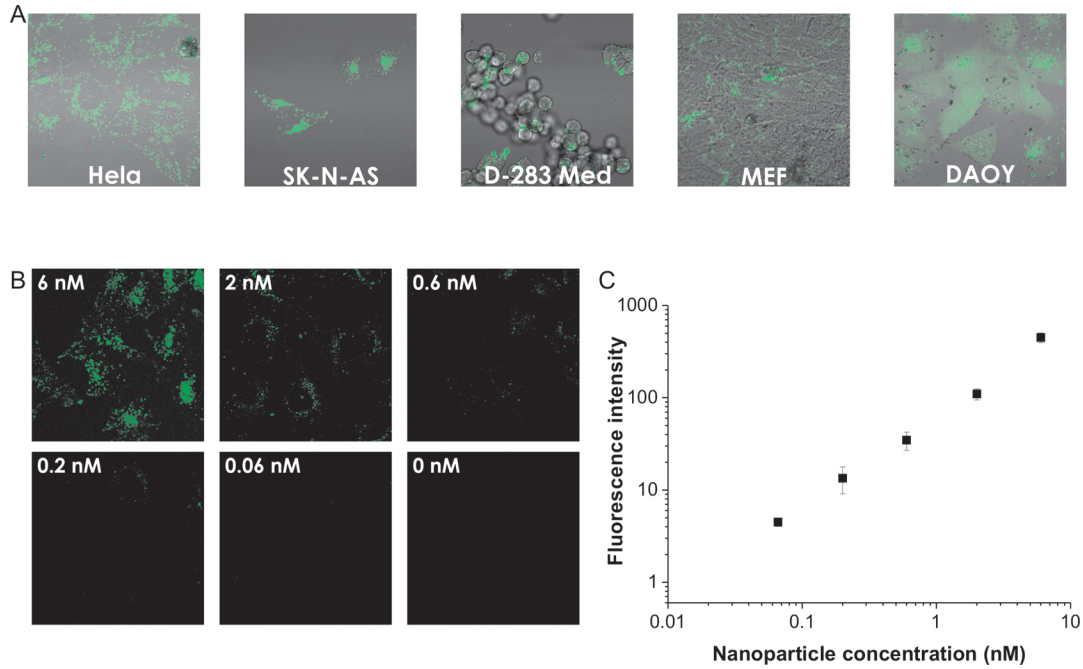

Figure 3. Intracellular fluorescence release as a quantitative indicator of the nanoparticles' endocytosis in various cell lines. (A) Different cell lines were incubated for 3 h with 6 nM of 5% CALNN-*th-fam*−95% CALNN gold nanoparticles. Fluorescence release was observed as previously described. From left to right: HeLa cells (human cervical cancer), SK-N-AS (human neuroblastoma), D-283 Med (human medulloblastoma), MEF (mouse embryonic fibroblasts), and DAOY (human medulloblastoma). (B,C) Fluorescence release is correlated with gold nanoparticle concentration in the medium. HeLa cells were incubated with increasing concentrations of 5% CALNN-*th-fam*−95% CALNN gold nanoparticles for 4 h and imaged as previously described. (C) Plot represents the quantification of mean single cell fluorescence intensity measured in ~50 cells for each nanoparticle concentration.

compared to the other cell lines. TEM confirmed that more nanoparticles were present in the endosomes (Supporting Information Figure S5) than what was observed for HeLa cells in similar conditions (Supporting Information Figure S1), suggesting that fluorescence unquenching could be used as a tool for quantitative comparisons of uptake between cell lines. This hypothesis was confirmed by a titration experiment in which HeLa cells were exposed to increasing concentration of nanoparticles showing a direct correlation between the level of fluorescence measured and the nanoparticle concentration (Figure 3B,C and flow cytometry Supporting Information Figure S6).

Two mechanisms could be responsible for the observed degradation of the peptide layer: (1) the peptides could be replaced by intracellular thiol-containing ligands through ligand exchange; (2) the peptides could be cleaved by proteolysis. To test the first hypothesis, we evaluated the effect of a second cysteine anchor on fluorescence release; the addition of a second cysteine should significantly reduce ligand exchange because of cooperative binding. No effect of the presence of a second cysteine could be detected (Figure 4A). Both type of particles entered the cells and lost the fluorescent label in identical proportions, indicating that ligand exchange is unlikely to be responsible for the observed peptide degradation and pointing toward proteolytic degradation.

The main enzymes in the acidic vesicles are the cathepsins, a family of peptidases that have very broad substrate specificity.[31] The main family members in acidic vesicles are B and L cathepsins. Cathepsin B degradation of peptide cargoes on cross-linked iron oxide (CLIO) nanoparticles has been reported previously in macrophages.[32] We confirmed that purified cathepsin L is able to cleave CALNN-*th-fam in vitro* using fluorescence unquenching, HPLC, and mass spectrometry (Supporting Information Figure S7). Nanoparticle uptake was imaged by live cell confocal microscopy in the presence of a cell-permeable irreversible cathepsin inhibitor (Z-FF-fmk, 20 μM) and in the presence or absence of 100 μM chloroquine. Cathepsin inhibition strongly impairs fluorescence release, demonstrating the involvement of cathepsin-dependent proteolytic activity in the degradation of the peptide layer (Figure 4B−F). We also observed an additive effect between Z-FF-fmk and chloroquine, with a 90% decrease of fluorescence in presence of both drugs together.

We monitored the fluorescence loss up to 24 h (cells were washed after 3 h to avoid chloroquine toxicity) and did not observe any further release of fluorescence due to the irreversible nature of the cathepsin inhibitor (not shown). Moreover, cells kept dividing and looked healthy in these conditions.

To eliminate the possibility that the variations in fluorescence could be due to variations in uptake induced by the drugs, we used direct imaging of the gold

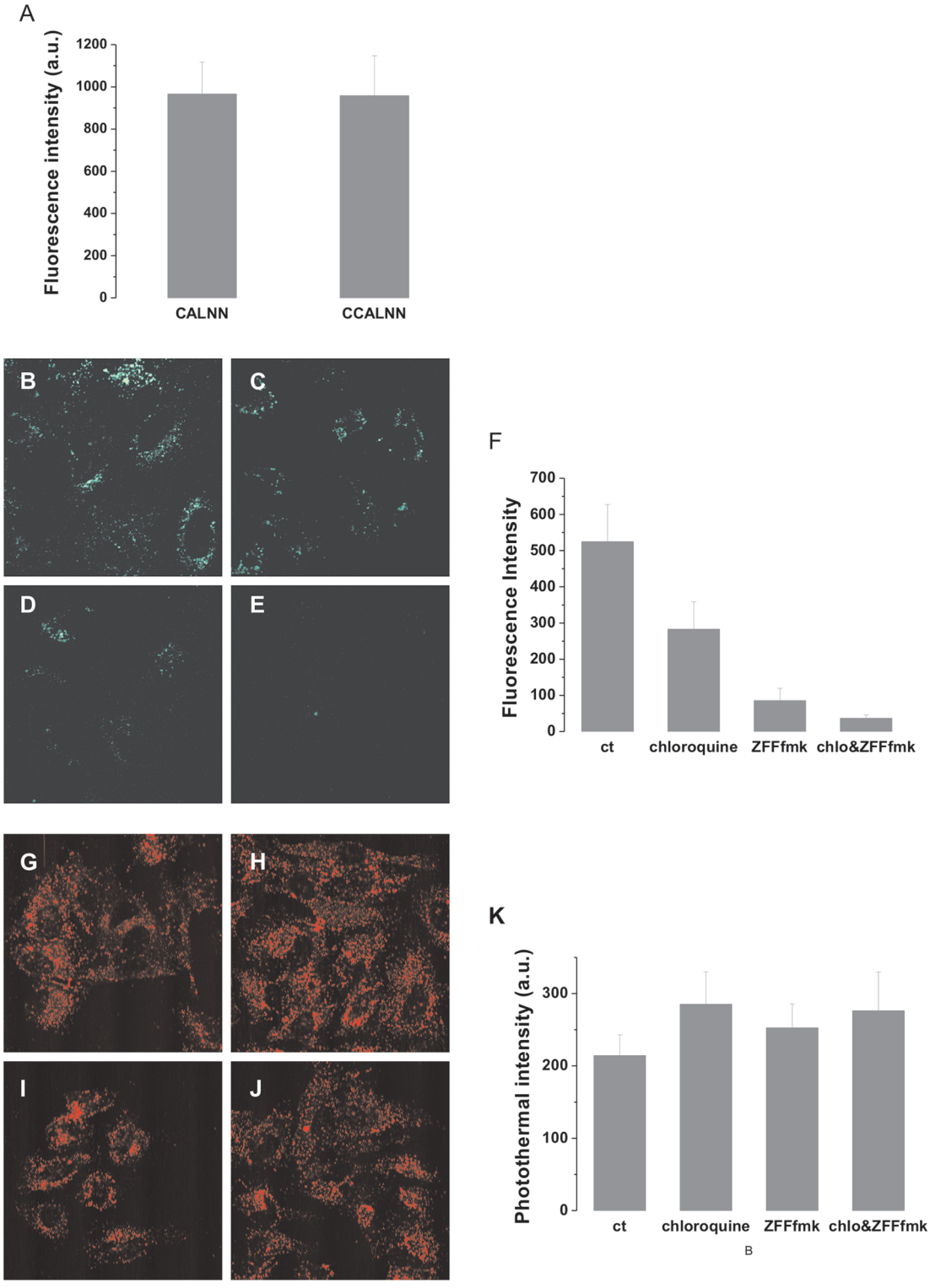

Figure 4. Cathepsin-dependent cleavage of the peptide monolayer. (A) HeLa cells were incubated for 4 h with 6 nM of 95% CALNN−5% CALNN-*th-fam* gold nanoparticles or 95% CCALNN−5% CCALNN-*th-fam* gold nanoparticles. Average number of fluorescent vesicles in ~200 cells was plotted for each condition. No statistical difference was observed between CALNN and CCALNN peptides. (B−E) Confocal images of fluorescence release inside cells after 4 h incubation with 6 nM of 95% CALNN−5% CALNN-*th-fam* gold nanoparticles. (B) Gold nanoparticles only, (C) gold nanoparticles in the presence of 100 μM chloroquine, (D) gold nanoparticles in the presence of 20 μM Z-FF-fmk (irreversible cathepsin inhibitor), (E) gold nanoparticles in the presence of both 100 μM chloroquine and 20 μM Z-FF-fmk. (F) Quantification of five different fields for each condition described in C−F. Average number of fluorescent vesicles/field is shown for each condition. (G−J) Photothermal images of nanoparticle uptake. (G) Gold nanoparticles only, (H) gold nanoparticles in the presence of 100 μM chloroquine, (I) gold nanoparticles in the presence of 20 μM Z-FF-fmk, (J) gold nanoparticles in the presence of both 100 μM chloroquine and 20 μM ZFF-fmk. (K) Quantification of photothermal intensity for each condition described in B−E. Average intensity of at least 40 cells is shown for each condition.

nanoparticles by photothermal microscopy. The photothermal signal is proportional to the number of nanoparticles in the focal point;[33] it therefore allows a direct comparison of the amount and localization of internalized gold nanoparticle in different conditions (see also photothermal titration, Supporting Information Figure S8). Figure 4G−J shows that the overall localization of the nanoparticles is not significantly affected; the nanoparticles do not appear to diffuse away from the broken endosomes. This is consistent with the TEM images (Supporting Information Figure S4) and could be attributed to the relatively large size of the nanoparticle, the very high density of intracellular medium, and the likely presence of unspecific interactions between the nanoparticles and intracellular macromolecules. Understanding the respective effects of these factors to allow the design and uptake of mobile nanoparticles will be the focus of further studies. The quantification of the photothermal images (Figure 4K) indicates that similar amounts of nanoparticles have been uptaken by the cells in the presence or absence of the drugs, confirming that the difference seen in fluorescence is not due to a difference in uptake but is rather due to the blocking of CALNN-*th-fam* degradation by the concerted action of chloroquine and Z-FF-fmk. The same combination of drugs impeded the degradation of the peptide CALNN-flag on nanoparticles, as shown by positive intracellular immunodetection (Supporting Information Figure S9). This is in line with the observed cathepsin-L-dependent CALNN-flag cleavage *in vitro* (HPLC and mass spectrometry Supporting Information Figure S10). Most intracellular applications of nanoparticles require the coupling of signal targeting peptides or/and of protein recognition domains or antibodies. We therefore examined which human proteins would be likely to be cleaved by the enzyme. On the basis of the literature,[34−36] a pattern defining the cathepsin L cleavage site was formulated. A search in the Uniprot database indicated

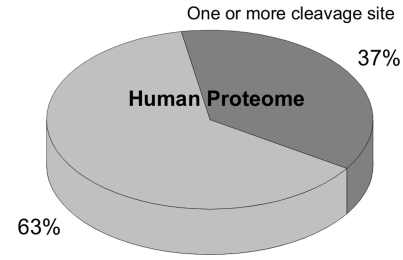

Figure 5. Cathepsin L potentially cuts a third of the human proteome. On the basis of the published literature,[34−36] a pattern, [WYFLASKH]-[AIKRH]-[FYVLI]-[KRH]-[VGNQSRHAFL]-[AVIGPNQSRHWYFLK]-[WYFLASNKHPD], defining the cathepsin L cleavage site was formulated by allowing at each substrate position any residue which gave a specificity constant (k_{cat}/K_m) of at least 10% of that of the most favored residue at that position. In a non-redundant set of 18 593 predicted human proteins (taken from Uniprot), around one-third (6875) were predicted to be cut at least once.

that more than a third of human proteins may be cut by cathepsin L (Figure 5); the full list of these proteins is given in Supporting Information (supporting Table 1). The implication is that the design of any intracellular nanodevice must take into account the possibility of cathepsin-L-induced degradation of sensing or targeting units.

CONCLUSION

We have shown that most nanomaterials conjugated with peptides and proteins are likely to get degraded during internalization if the nanoparticles transit through endosomal compartments. This observation has immediate consequences for biosensing. Entry mechanisms that bypass the endosomal pathway have been proposed. It is now important for the progress of the field that such pathways can be compared and evaluated. In future studies, success should be assessed by the breakdown of the correlation between intra-endosomal proteolytic cleavage and nanoparticle entry, both of which can be measured quantitatively.

MATERIALS AND METHODS

Reagents and Antibodies. Tissue culture medium was from Gibco Life Technologies (Carlsbad, Ca); fetal calf serum (FCS) from Harlan Seralab (UK); pharmacological inhibitor Z-FF-fmk from Calbiochem (EMD Biosciences, Germany). Gold nanoparticles were from BBInternational (Cardiff, UK). Peptides were from Anaspec (San Jose, CA) and PPR Ltd. (Fareham, UK). Purified human cathepsin L, purified bovine thrombin, choloroquine, 3-methyladenine (3-MA), antibody to FLAG epitope, and secondary Cy3-conjugated antimouse antibody were from Sigma (St. Louis, MO).

Peptide Stock Solutions. A 2 mM stock solution of CALNN was prepared by dissolving it in concentrated phosphate buffer saline (10× PBS; 1.6 M NaCl, 30 mM KCl, 80 mM Na_2HPO_4, 10 mM KH_2PO_4).

The stock solutions of the peptides CALNNGGDYKAFDNL (CALNN-*flag*), CCALNNGGGALVPRGSGTAK(5 carboxyfluorescein)-NH_2 (CALNN-*th-fam*), CCALNNGGGALVPRGSGTAK(5-carboxy-fluorescein)-NH_2 (CCALNN-*th-fam*) were prepared by dissolving them in dimethyl sulfoxide. The resulting solutions were kept as aliquots at −80 °C.

Formation of Peptide Self-Assembled Monolayers. A peptide solution was prepared by mixing the above stock solutions in the appropriate volume ratio. The peptide solution was mixed in a 1:1 ratio with 10× PBS (see composition above). A suspension of 10 nm diameter gold nanoparticles (BBInternational, Cardiff, UK) was added in a 9:1 volume ratio giving a 100 μM final concentration of peptide. The solution was briefly agitated before addition of Tween-20 to a final concentration of 0.05% (v/v). The solutions were left overnight at room temperature in the dark to avoid photobleaching of the fluorophores.

Purification Procedure. The nanoparticle solutions were centrifuged (16 000*g*, 60 min), and the pellet was resuspended in 1 mL of phosphate buffer saline (PBS; 160 mM NaCl, 3 mM KCl, 8 mM Na_2HPO_4, 1 mM KH_2PO_4) with 0.05% Tween-20 before a second centrifugation step (16 000*g*, 60 min). This washing step was repeated three times with PBS only, before resuspension in PBS at a final nanoparticle concentration of 60 nM. Successful formation of the monolayer is immediately visible because of the increased colloidal stability and of a small red shift of the plasmon band.[20] The repeated centrifugation procedure ensures that

the concentration of excess free peptide is in the picomolar range.

Cell Culture. HeLa cells were grown in Dulbecco's modified Eagle's medium (DMEM) supplemented with 10% FCS (v/v) and 1% non-essential amino acids (v/v), at 37 °C, 5% CO_2. Cells (between passages 8 to 20) were plated at 1.105 cells/mL. For all experiments, nanoparticles were incubated directly into the complete medium (containing 10% FCS) for indicated times at a final concentration of 6 nM or otherwise stated.

Lysotracker. Lysotracker Red-DND 99 (InVitrogen-Molecular Probes, Carlsbad, CA) was incubated 15 min on cells (final concentration 37 nM), and the excess of dye was then washed out before imaging on a LSM510 confocal microscope. Excitation was performed using a green helium−neon laser (543 nm) and detected through both a 545 nm dichroic mirror and a 560 nm long-pass filter.

Confocal Microscopy. ***Time Lapse.*** Cells were plated in 35 mm glass coverslip culture dishes (Iwaki). One day after plating, cells were then incubated on the microscope stage at 37 °C, 5% CO_2, and observed by confocal microscopy using a Zeiss LSM510 with a Plan-apochromat 63× 1.3 NA oil immersion objective. Excitation of fluorescein was performed using an argon ion laser at 488 nm. Emitted light was detected through a 505−550 nm bandpass filter from a 545 nm dichroic mirror. Data capture was carried out with LSM510 version 3 software (Zeiss, Germany). For time-lapse experiments, mean fluorescence intensity was extracted and the fluorescence intensity relative to starting fluorescence was determined for each cell using LSM510 software. These experiments were performed at least three times, and each time, eight different fields which each contain ~5−10 cells were analyzed.

Statistical Analysis. For fluorescence intensity quantification, 10 images containing each ~20 cells were taken for each condition. Number of fluorescent vesicles was then counted for each field as well as mean fluorescence intensity for each individual cell using kinetic tracking analysis software (2002 Kinetic Imaging, Ltd.). Histograms represent the mean values ± SD. Statistical significance was determined by one-way ANOVA followed by a Bonferroni multiple comparison test. Difference was considered as significant at $p < 0.01$. All of these experiments were performed at least three times.

Transmission Electron Microscopy. Cells were plated at 2.105 cells/mL in a 35 mm Petri dish. One day after plating, cells were incubated for 3 h with 6 nM (final) nanoparticles. After one PBS wash, cells were fixed with 4% paraformaldehyde and 2% glutaraldehyde in 0.1 M phosphate buffer solution, osmicated, and processed for epoxy resin embedding. Then, 70 nm sections were cut with a LKB ultramichrotome and stained with 5% aqueous uranyl acetate and 2% lead citrate before viewing in a FEI Tecnai Spirit transmission electron microscope.

***In Vitro* Fluorescence Assay.** For thrombin cleavage, each reaction (100 μL) was performed in PBS with 0.3 M NaCl (pH 7.4), with 6 nM of 98% CALNN−2% CALNN-*th-fam* nanoparticles and 50 mU of purified thrombin. Fluorescence was measured using a BMG labtech POLARstar fluorimeter (Offenburg, Germany) and Corning (Corning Inc., NY) black NBS plates.

Photothermal Microscopy. Following confocal microscopy imaging, the cells were fixed and observed by photothermal heterodyne microscopy 33 in 35 mm glass coverslip culture dishes (Iwaki). The absorbing beam (523 nm, Nd:YAG frequency doubled laser) modulated at the frequency ω ($\omega/2\pi = 692.5$ kHz) by an acousto-optic modulator and the probe beam (632.8 nm, HeNe laser) were focused on the sample using a Zeiss Achroplan 50× 0.9 NA oil immersion objective. The beam's intensities were, respectively, 0.44 and 10.65 mW. The forward interfering fields were collected with a Zeiss Achroplan 40× 0.8 NA water dipping objective and sent on a photodiode. The beat signal at the frequency ω was extracted *via* a lock-in amplifier and integrated over 10 ms. All images were completed by moving the sample with a piezo-electric device (Physik Instrumente) over the fixed laser beams and were taken at the altitude of 1 μm above the glass coverslip surface.

Statistical Analysis. The photothermal signal of an image was measured by taking the mean photothermal signal above a threshold (1.5 times the background mean intensity of cells without NPs) for all of the cells fully included in the field (checked with the corresponding brightfield image). The analysis was performed using Kinetic Tracking Analysis software (2002 Kinetic Imaging, Ltd.). Approximately 10 cells were present on each field, and at least 40 cells on at least three different fields were analyzed per condition.

Acknowledgment. We acknowledge funding from the Biotechnology and Biological Sciences Research Council (BBSRC, Technology Development Research Initiative, BBE0042101). V.S. and R.L. are BBSRC David Phillips fellows (BBC5204711, BBD0206381). I.A.P. is a Royal Society University Research fellow. We thank A. Beckett for electron microscopy assistance, A. Ori for assistance with HPLC, and J. Grant and J. Wong for technical support.

Supporting Information Available: Confocal fluorescence of nanoparticle entry and degradation in cells (movie); list of proteins potentially degraded by cathepsin L from Uniprot (supplemental table); additional figures as cited in the text: TEM, immunofluorescence, HPLC, *in vitro* controls, and photothermal microscopy quantification. This material is available free of charge *via* the Internet at http://pubs.acs.org.

REFERENCES AND NOTES

1. Selhuber-Unkel, C.; Zins, I.; Schubert, O.; Sonnichsen, C.; Oddershede, L. B. Quantitative Optical Trapping of Single Gold Nanorods. *Nano Lett.* **2008**, *8*, 2998–3003.
2. Lasne, D.; Blab, G. A.; Berciaud, S.; Heine, M.; Groc, L.; Choquet, D.; Cognet, L.; Lounis, B. Single Nanoparticle Photothermal Tracking (SNaPT) of 5-nm Gold Beads in Live Cells. *Biophys. J.* **2006**, *91*, 4598–4604.
3. Courty, S.; Luccardini, C.; Bellaiche, Y.; Cappello, G.; Dahan, M. Tracking Individual Kinesin Motors in Living Cells Using Single Quantum-Dot Imaging. *Nano Lett.* **2006**, *6*, 1491–1495.
4. Boyer, D.; Tamarat, P.; Maali, A.; Lounis, B.; Orrit, M. Photothermal Imaging of Nanometer-Sized Metal Particles Among Scatterers. *Science* **2002**, *297*, 1160–1163.
5. Skala, M. C.; Crow, M. J.; Wax, A.; Izatt, J. A. Photothermal Optical Coherence Tomography of Epidermal Growth Factor Receptor in Live Cells Using Immunotargeted Gold Nanospheres. *Nano Lett.* **2008**, *8*, 3461–3467.
6. Lindfors, K.; Kalkbrenner, T.; Stoller, P.; Sandoghdar, V. Detection and Spectroscopy of Gold Nanoparticles Using Supercontinuum White Light Confocal Microscopy. *Phys. Rev. Lett.* **2004**, *93*, 037401.
7. Hell, S. W. Far-Field Optical Nanoscopy. *Science* **2007**, *316*, 1153–1158.
8. Sperling, R. A.; Gil, P. R.; Zhang, F.; Zanella, M.; Parak, W. J. Biological Applications of Gold Nanoparticles. *Chem. Soc. Rev.* **2008**, *37*, 1896–1908.
9. Khan, J. A.; Pillai, B.; Das, T. K.; Singh, Y.; Maiti, S. Molecular Effects of Uptake of Gold Nanoparticles in HeLa Cells. *ChemBioChem* **2007**, *8*, 1237–1240.
10. Pan, Y.; Neuss, S.; Leifert, A.; Fischler, M.; Wen, F.; Simon, U.; Schmid, G.; Brandau, W.; Jahnen-Dechent, W. Size-Dependent Cytotoxicity of Gold Nanoparticles. *Small* **2007**, *3*, 1941–1949.
11. Tsoli, M.; Kuhn, H.; Brandau, W.; Esche, H.; Schmid, G. Cellular Uptake and Toxicity of Au(55) Clusters. *Small* **2005**, *1*, 841–844.
12. Liu, Y. L.; Shipton, M. K.; Ryan, J.; Kaufman, E. D.; Franzen, S.; Feldheim, D. L. Synthesis, Stability, and Cellular Internalization of Gold Nanoparticles Containing Mixed Peptidepoly(ethylene glycol) Monolayers. *Anal. Chem.* **2007**, *79*, 2221–2229.
13. Nativo, P.; Prior, I. A.; Brust, M. Uptake and Intracellular Fate of Surface-Modified Gold Nanoparticles. *ACS Nano* **2008**, *2*, 1639–1644.
14. Verma, A.; Uzun, O.; Hu, Y. H.; Hu, Y.; Han, H. S.; Watson, N.; Chen, S. L.; Irvine, D. J.; Stellacci, F. Surface-Structure-Regulated Cell-Membrane Penetration by Monolayer-Protected Nanoparticles. *Nat. Mater.* **2008**, *7*, 588–595.

15. Chithrani, B. D.; Chan, W. C. W. Elucidating the Mechanism of Cellular Uptake and Removal of Protein-Coated Gold Nanoparticles of Different Sizes and Shapes. *Nano Lett.* **2007**, *7*, 1542–1550.
16. Ryan, J. A.; Overton, K. W.; Speight, M. E.; Oldenburg, C. M.; Loo, L.; Robarge, W.; Franzen, S.; Feldheim, D. L. Cellular Uptake of Gold Nanoparticles Passivated with BSA-SV40 Large T Antigen Conjugates. *Anal. Chem.* **2007**, *79*, 9150–9159.
17. Hong, R.; Han, G.; Fernandez, J. M.; Kim, B. J.; Forbes, N. S.; Rotello, V. M. Glutathione-Mediated Delivery and Release Using Monolayer Protected Nanoparticle Carriers. *J. Am. Chem. Soc.* **2006**, *128*, 1078–1079.
18. Han, G.; Chari, N. S.; Verma, A.; Hong, R.; Martin, C. T.; Rotello, V. M. Controlled Recovery of the Transcription of Nanoparticle-Bound DNA by Intracellular Concentrations of Glutathione. *Bioconjugate Chem.* **2005**, *16*, 1356–1359.
19. Levy, R. Peptide-Capped Gold Nanoparticles: Towards Artificial Proteins. *ChemBioChem* **2006**, *7*, 1141–1145.
20. Levy, R.; Thanh, N. T. K.; Doty, R. C.; Hussain, I.; Nichols, R. J.; Schiffrin, D. J.; Brust, M.; Fernig, D. G. Rational and Combinatorial Design of Peptide Capping Ligands for Gold Nanoparticles. *J. Am. Chem. Soc.* **2004**, *126*, 10076–10084.
21. Doty, R. C.; Tshikhudo, T. R.; Brust, M.; Fernig, D. G. Extremely Stable Water-Soluble Ag Nanoparticles. *Chem. Mater.* **2005**, *17*, 4630–4635.
22. Michalet, X.; Pinaud, F. F.; Bentolila, L. A.; Tsay, J. M.; Doose, S.; Li, J. J.; Sundaresan, G.; Wu, A. M.; Gambhir, S. S.; Weiss, S. Quantum Dots for Live Cells, *In Vivo* Imaging, and Diagnostics. *Science* **2005**, *307*, 538–544.
23. Sarikaya, M.; Tamerler, C.; Jen, A. K. Y.; Schulten, K.; Baneyx, F. Molecular Biomimetics: Nanotechnology through Biology. *Nat. Mater.* **2003**, *2*, 577–585.
24. Kuhn, S.; Hakanson, U.; Rogobete, L.; Sandoghdar, V. Enhancement of Single Molecule Fluorescence Using a Gold Nanoparticle as an Optical Nanoantenna. *Phys. Rev. Lett.* **2006**, *97*, 017402.
25. Dulkeith, E.; Ringler, M.; Klar, T. A.; Feldmann, J.; Javier, A. M.; Parak, W. J. Gold Nanoparticles Quench Fluorescence by Phase Induced Radiative Rate Suppression. *Nano Lett.* **2005**, *5*, 585–589.
26. Lee, S.; Cha, E. J.; Park, K.; Lee, S. Y.; Hong, J. K.; Sun, I. C.; Kim, S. Y.; Choi, K.; Kwon, I. C.; Kim, K.; Ahn, C. H. A Near-Infrared-Fluorescence-Quenched Gold-Nanoparticle Imaging Probe for *In Vivo* Drug Screening and Protease Activity Determination. *Angew. Chem., Int. Ed.* **2008**, *47*, 2804–2807.
27. Seglen, P. O.; Grinde, B.; Solheim, A. E. Inhibition of the Lysosomal Pathway of Protein-Degradation in Isolated Rat Hepatocytes by Ammonia, Methylamine, Chloroquine and Leupeptin. *Eur. J. Biochem.* **1979**, *95*, 215–225.
28. Wadia, J. S.; Stan, R. V.; Dowdy, S. F. Transducible TAT-HA Fusogenic Peptide Enhances Escape of TAT-Fusion Proteins after Lipid Raft Macropinocytosis. *Nat. Med.* **2004**, *10*, 310–315.
29. Sandhu, K. K.; McIntosh, C. M.; Simard, J. M.; Smith, S. W.; Rotello, V. M. Gold Nanoparticle-Mediated Transfection of Mammalian Cells. *Bioconjugate Chem.* **2002**, *13*, 3–6.
30. Seleverstov, O.; Phang, J. M.; Zabirnyk, O. Semiconductor Nanocrystals in Autophagy Research: Methodology Improvement at Nanosized Scale. *Methods Enzymol.* **2009**, *452*, 277–296.
31. Pillay, C. S.; Elliott, E.; Dennison, C. Endolysosomal Proteolysis and Its Regulation. *Biochem. J.* **2002**, *363*, 417–429.
32. Kircher, M. F.; Weissleder, R.; Josephson, L. A Dual Fluorochrome Probe for Imaging Proteases. *Bioconjugate Chem.* **2004**, *15*, 242–248.
33. Berciaud, S.; Cognet, L.; Blab, G. A.; Lounis, B. Photothermal Heterodyne Imaging of Individual Non-fluorescent Nanoclusters and Nanocrystals. *Phys. Rev. Lett.* **2004**, *93*, 257402.
34. Puzer, L.; Cotrin, S. S.; Alves, M. F. M.; Egborge, T.; Araujo, M. S.; Juliano, M. A.; Juliano, L.; Bromme, D.; Carmona, A. K. Comparative Substrate Specificity Analysis of Recombinant Human Cathepsin V and Cathepsin L. *Arch. Biochem. Biophys.* **2004**, *430*, 274–283.
35. Portaro, F. C. V.; Santos, A. B. F.; Cezari, M. H. S.; Juliano, M. A.; Juliano, L.; Carmona, E. Probing the Specificity of Cysteine Proteinases at Subsites Remote from the Active Site: Analysis of P-4, P-3, P-2′ and P-3′ Variations in Extended Substrates. *Biochem. J.* **2000**, *347*, 123–129.
36. Menard, R.; Carmona, E.; Plouffe, C.; Bromme, D.; Konishi, Y.; Lefebvre, J.; Storer, A. C. The Specificity of the S(1)′ Subsite of Cysteine Proteases. *FEBS Lett.* **1993**, *328*, 107–110.